JOURNAL OF NANOMATERIALS AND APPLICATIONS

Journal of Nanomaterials and Applications

Journal homepage: https://jna.com.vn

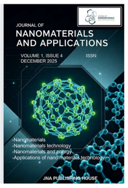

First-principles investigation of structural, electronic and optical properties of rhombohedral $Na_{0.5}Bi_{0.5}TiO_3$

Duong Quoc Van[1,*], Le Minh Thu[2], Ştefan Ţălu [3,*]

[1,2,] Faculty of Physics, Hanoi National University of Education, 136 Xuan Thuy, Cau Giay, 100000, HaNoi, Vietnam.

[3,] Technical University of Cluj-Napoca, The Directorate of Research, Development and Innovation Management, Constantin Daicoviciu Street, no. 15, Cluj-Napoca, 400020, Cluj county, Romania.

Article info

Type of articles:

Original research paper

Corresponding author*:

Duong Quoc Van:
vandq@hnue.edu.vn
Ştefan Ţălu:
stefan_ta@yahoo.com

Received: 29 December 2025
Revised: 31 January 2026
Accepted: 07 February 2026
Published: 28 March 2026

Abstract: Rhombohedral $Na_{0.5}Bi_{0.5}TiO_3$ (NBT) is a representative lead-free ferroelectric, yet a unified microscopic understanding linking bonding, electronic structure, and optical response remains incomplete. In this work, first-principles density functional theory calculations are performed to systematically investigate the structural, electronic, magnetic, and optical properties of pristine rhombohedral NBT. The optimized R3c structure is energetically stable and consistent with experimental data. Electronic structure analysis shows that NBT is a direct band-gap semiconductor with a calculated gap of ~2.86 eV, where the valence band is dominated by O-2p states and the conduction band mainly originates from Ti-3d states with minor Bi-6p contributions. Mulliken population analysis reveals a mixed ionic–covalent bonding nature, with pronounced Ti–O covalency. Importantly, a clear correlation between Ti–O covalent interactions, conduction-band formation, and dominant ultraviolet optical transitions is established, providing a quantitative microscopic interpretation beyond previous qualitative studies. Spin-polarized calculations confirm an intrinsically non-magnetic ground state. These results offer a reliable theoretical reference for NBT-based functional materials.

Keywords: $Na_{0.5}Bi_{0.5}TiO_3$; lead-free ferroelectrics; electronic structure; optical response; first-principle calculations

---

1. Introduction

Sodium bismuth titanate, $Na_{0.5}Bi_{0.5}TiO_3$ (NBT), is a representative lead-free ferroelectric material that has attracted significant attention as a potential alternative to Pb-based perovskites in environmentally friendly electronic and electromechanical applications.

Recent atomistic simulations based on first-principles methods have demonstrated their effectiveness in linking atomic bonding to electronic and optical properties, providing a reliable theoretical framework for materials analysis and prediction [1].

Since its discovery by Smolenskii *et al.* in the early 1960s [2], NBT has been extensively studied due to its high Curie temperature, large remanent polarization, and chemical stability. Structurally, NBT crystallizes in a perovskite ABO_3 framework with a random distribution of Na^+ and Bi^{3+} cations at the A-site. Depending on temperature, NBT undergoes a sequence of structural phase transitions, exhibiting a cubic phase at high temperatures, a tetragonal phase at intermediate temperatures, and a rhombohedral R3c phase at room temperature [3,4].

Among these phases, the rhombohedral phase is of particular interest because it governs the intrinsic ferroelectric, dielectric, and optical properties of NBT under ambient conditions. Experimentally, rhombohedral NBT ceramics exhibit a relatively large remanent polarization and coercive field, but a modest piezoelectric coefficient compared to Pb-based counterparts [5,6]. Consequently, extensive efforts have been devoted to improving the functional performance of NBT through compositional modification, solid-solution design, and microstructural engineering [7–13]. In parallel, a wide range of experimental studies have explored the structural characteristics, phase transitions, vibrational spectra, dielectric response, and optical behavior of pristine and modified NBT systems [14–19]. From a theoretical perspective, first-principles density functional theory (DFT) calculations have played an essential role in elucidating the microscopic origin of NBT's physical properties. Previous studies using different computational frameworks, such as WIEN2k, VASP, Quantum ESPRESSO, and CASTEP, have reported the electronic band structure, density of states, and selected optical properties of NBT in its various crystallographic phases [20–24]. These works consistently indicate that rhombohedral NBT is a wide-band-gap semiconductor, with valence bands dominated by O-2p states and conduction bands primarily derived from Ti-3d and Bi-related states. Optical spectra calculated from first-principles have also provided useful insights into the absorption edge and dielectric response of the material.

Despite extensive experimental and theoretical investigations, a critical limitation of previous first-principles studies on pristine rhombohedral $Na_{0.5}Bi_{0.5}TiO_3$ lies in the absence of a quantitative and unified correlation between chemical bonding characteristics, electronic band-edge formation, and optical transition mechanisms. Although Ti–O hybridization has frequently been mentioned in earlier reports, it has mainly been discussed in a qualitative manner without explicit linkage to conduction-band composition or specific features in the calculated optical spectra. In particular, the relationship between bond population analysis, orbital-resolved density of states near the band edges, and the energy positions of dominant dielectric-function peaks remains insufficiently clarified. As a result, a coherent microscopic picture connecting structure, bonding, and optical response in pristine rhombohedral NBT is still lacking.

In this work, we present a comprehensive first-principles study of rhombohedral $Na_{0.5}Bi_{0.5}TiO_3$ with a particular emphasis on establishing a quantitative and explicit correlation between chemical bonding, electronic band-edge formation, and optical transition mechanisms within a single and consistent computational framework. Particular emphasis is placed on establishing a quantitative correlation between partial density of states, Mulliken population analysis, and optical transition mechanisms. By explicitly linking Ti–O covalent interactions to conduction-band formation and dominant ultraviolet optical excitations, this study provides a coherent microscopic interpretation that goes beyond previous isolated electronic or optical analyses. The results offer a reliable theoretical reference for understanding pristine NBT and for future studies on modified NBT-based materials.

2. Computational Details

First-principles calculations were performed within the framework of density functional theory (DFT) using the Cambridge Serial Total Energy Package (CASTEP) as implemented in the Materials Studio software package [25]. The rhombohedral R3c structure of $Na_{0.5}Bi_{0.5}TiO_3$ was adopted as the initial model, with experimental lattice parameters reported by Jones *et al.* [26]. The unit cell contains 30 atoms, including 3 Bi, 3 Na, 6 Ti, and 18 O atoms. The exchange–correlation effects were treated using the generalized gradient approximation (GGA) with the Perdew–Burke–Ernzerhof (PBE) functional [27,28]. Electron–ion interactions were described by Vanderbilt ultrasoft pseudopotentials [29], with the following valence configurations: Bi ($6s^2 6p^3$), Na ($3s^1$), Ti ($3d^2 4s^2$), and O ($2s^2 2p^4$). A plane-wave cutoff energy of 410 eV was employed for all calculations. Structural optimization was carried out using the Broyden–Fletcher–Goldfarb–Shanno (BFGS) algorithm [30–33] until the convergence criteria were satisfied. The thresholds for total energy, maximum force, maximum stress, and maximum atomic displacement were set to 5×10^{-6} eV/atom, 1×10^{-2} eV/Å, 2×10^{-2} GPa, and 5×10^{-4} Å, respectively. For electronic structure calculations, a stricter total energy convergence criterion of 5×10^{-7} eV was applied. Brillouin-zone integrations were performed using a 6×6×6 Monkhorst–Pack k-point mesh [34], corresponding to 38 k-points in the irreducible Brillouin zone. Spin-polarized calculations were conducted to examine the possible magnetic behavior of pristine $Na_{0.5}Bi_{0.5}TiO_3$, although no external magnetic field, defects, or dopants were introduced. Optical properties, including the dielectric function, absorption coefficient, reflectivity, refractive index, optical conductivity, and energy-loss function, were calculated based on the linear response formalism using the optimized ground-state electronic structure. Although hybrid functionals or modified Becke–Johnson (mBJ) approaches may yield improved absolute band-gap values, the PBE functional was adopted in this work to ensure consistency with a wide range of previous first-principles studies on NBT and to reliably capture relative trends in electronic structure and optical transitions. Since the primary objective of this study is to establish quantitative correlations between structure, chemical bonding, and optical response rather than absolute band-gap correction, the PBE framework is considered appropriate. Although Mulliken population analysis is known to be basis-set dependent, it remains a useful and widely adopted tool for comparative bonding analysis when applied consistently within the same computational framework, as adopted in the present work.

3. Results and Discussion

3.1 Structural Properties

Accurate determination of the equilibrium crystal structure is a prerequisite for reliable prediction of the electronic and optical properties of crystalline materials. Therefore, full geometry optimization of rhombohedral $Na_{0.5}Bi_{0.5}TiO_3$ was first performed to obtain the energetically stable configuration. The total energy of the unit cell converged smoothly with respect to the optimization steps, reaching a minimum after approximately 30 iterations, which indicates good convergence and structural stability of the optimized configuration. Figure 1 shows the convergence behavior of the total energy during structural optimization.

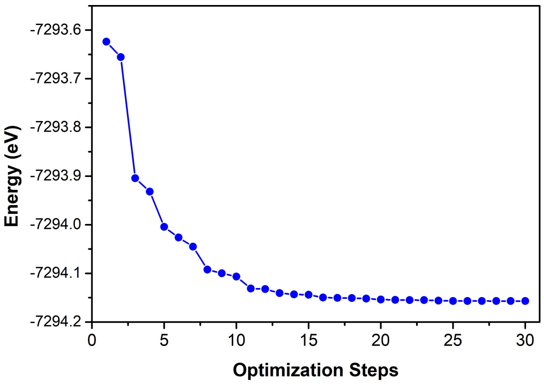

Figure 1. Minimized final energy converges through the calculated iterations of NBT.

The optimized crystal structure preserves the rhombohedral R3c symmetry and exhibits a characteristic distortion relative to the ideal cubic perovskite structure. This distortion is manifested by a slight elongation along the crystallographic c-axis and off-center displacements of both A-site and B-site cations. Such structural features are commonly associated with the stereochemical activity of Bi $6s^2$ lone-pair electrons, which induce local asymmetry and stabilize the ferroelectric rhombohedral phase at room temperature. This intrinsic distortion plays a crucial role in determining the bonding characteristics, electronic band dispersion, and anisotropic optical response of NBT.

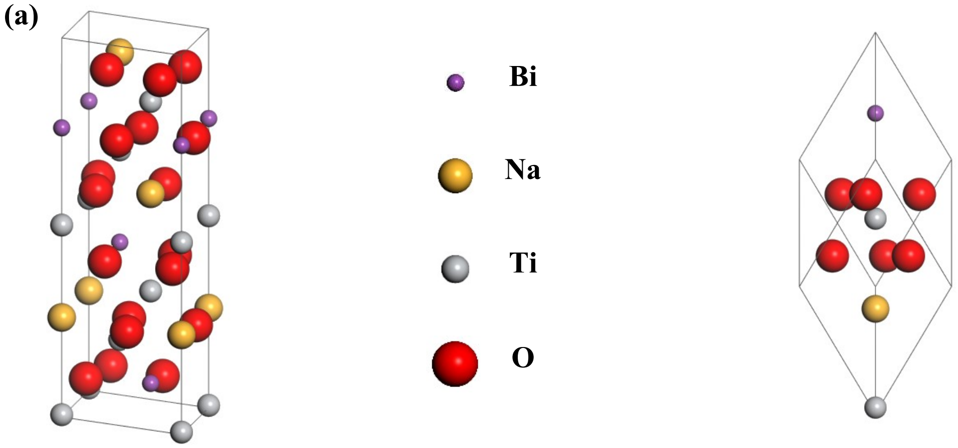

Figure 2. Optimized crystal structure of rhombohedral $Na_{0.5}Bi_{0.5}TiO_3$: (a) conventional unit cell and (b) primitive cell.

Figure 2 Illustrates the optimized crystal structure of NBT, including both the conventional unit cell and the corresponding primitive cell. The unit cell contains 30 atoms (3 Bi, 3 Na, 6 Ti, and 18 O atoms), whereas the primitive cell consists of 10 atoms (1 Bi, 1 Na, 2 Ti, and 6 O atoms). The calculated lattice parameters of the optimized unit cell are a = b = 5.4939 Å and c = 13.8345 Å, which are in good agreement with available experimental data [26] and previous first-principles calculations [35]. The small deviations from experimental values are typical for GGA-PBE calculations and do not affect the qualitative description of the structural and electronic properties. For a more detailed structural comparison, the lattice parameters and atomic positions of the primitive cell were also analyzed. The obtained rhombohedral lattice constants and rhombohedral angle are consistent with experimental reports and earlier theoretical studies [20,21,24]. Table 1 summarizes the fractional atomic coordinates of Bi/Na, Ti, and O atoms in the primitive cell, showing good agreement with both experimental data [26] and prior first-principles results [20]. Minor differences in atomic positions can be attributed to the choice of exchange–correlation functional and computational parameters. Table 1 summarizes the fractional atomic coordinates.

Table 1. Structure of NBT material.

Sites	**x**	**y**	**z**	**Reference**
Bi/Na	0.2644	0.2644	0.2644	This work
	0.2699	0.2699	0.2699	Calculated [20]
	0.2627	0.2627	0.2627	Experiment [26]
Ti	0.0080	0.0080	0.0080	This work
	0.0123	0.0123	0.0123	Calculated [20]
	0.0063	0.0063	0.0063	Experiment [26]
O	0.2110	0.2950	0.7491	This work
	0.1814	0.3138	0.7447	Calculated [20]
	0.2093	0.2093	0.7473	Experiment [26]

Overall, the optimized structural parameters confirm that the adopted computational setup reliably reproduces the intrinsic rhombohedral distortion of $Na_{0.5}Bi_{0.5}TiO_3$. This optimized structure serves as a robust basis for subsequent analyses of electronic structure, chemical bonding, and optical properties. In particular, the local distortion of TiO_6 octahedra and the off-center displacement of cations are expected to strongly influence Ti–O hybridization, which will be discussed in detail in the following sections.

3.2 Electronic Structures

To elucidate the intrinsic electronic properties of rhombohedral $Na_{0.5}Bi_{0.5}TiO_3$, electronic structure calculations were performed based on the optimized primitive cell shown in Figure 2(b), which significantly reduces computational cost while preserving the essential structural characteristics. Figure 3a presents the Brillouin zone of the rhombohedral phase together with the selected high-symmetry k-path used for band-structure calculations. The band dispersion was evaluated along the Γ–F–Z path, which adequately captures the critical features near the band edges. The calculated electronic band structure of pristine NBT is shown in Figure 3b.

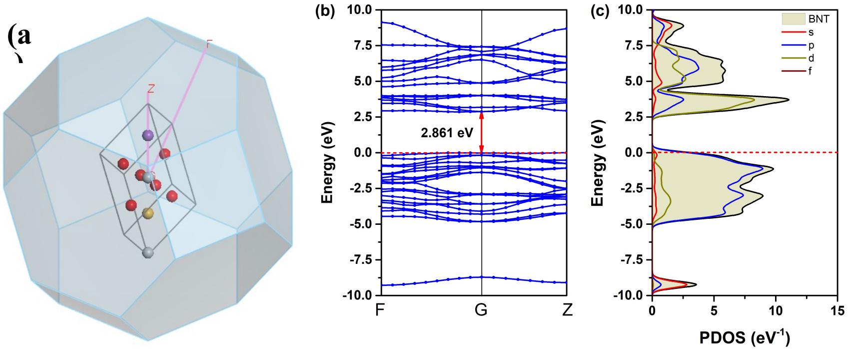

Figure 3. Brillouin zone (a), band structures (b) and partial density of states (PDOS) (c) of NBT.

It is evident that NBT exhibits a direct band-gap semiconducting character, with both the valence-band maximum (VBM) and the conduction-band minimum (CBM) located at the same k-point. The calculated band-gap value is approximately 2.86 eV, which is consistent with previous first-principles studies [20,21,24,36] and reasonably close to experimental estimates when considering the well-known band-gap underestimation of the GGA-PBE functional.

It should be noted that the calculated electronic band gap is smaller than the optical band gap extracted from absorption spectra, which is a common feature in wide-band-gap oxides. This difference arises from excitonic effects, optical transition matrix elements, and the intrinsic underestimation of band gaps within the GGA-PBE framework, as well as the fact that optical measurements probe vertical transitions rather than fundamental electronic gaps.

The Fermi level is located at the top of the valence band, further confirming the intrinsic semiconducting nature of rhombohedral NBT. To gain deeper insight into the orbital origin of the electronic bands, the total and partial densities of states (DOS and PDOS) are presented in Figure 3c. The electronic states can be broadly divided into three energy regions. The valence band, extending from approximately −5.0 eV to 0 eV, is dominated by O-2p states with significant hybridization with Ti-3d orbitals. The conduction band, starting from about 2.5 eV above the Fermi level, mainly consists of Ti-3d states with additional contributions from Bi-6p orbitals at higher energies. A deeper bonding region around −9 to −10 eV is primarily associated with Bi-6s–O-2p hybridization, reflecting the stereochemically active lone-pair character of Bi. The strong hybridization between Ti-3d and O-2p states near both the VBM and CBM indicates pronounced Ti–O covalency, which plays a decisive role in determining the electronic band dispersion and the direct nature of the band gap. This covalent interaction enhances orbital overlap within the TiO_6 octahedra, leading to increased band dispersion near the band edges and facilitating direct optical transitions. In contrast, Bi-6p states mainly contribute to higher-energy conduction bands, suggesting a secondary role in low-energy electronic excitations.

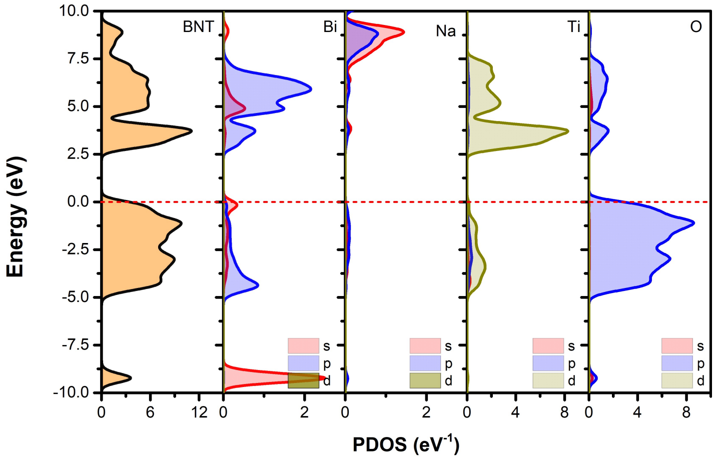

Figure 4. Density of states (DOS) and the contributions of elements in NBT.

Figure 4 further resolves the elemental contributions to the DOS, confirming that the electronic structure near the band gap is primarily governed by the TiO_6 octahedral framework. While Bi and Na atoms are essential for structural stabilization and charge balance, their direct contribution to the electronic states near the Fermi level is relatively limited compared to that of Ti and O. This observation highlights the dominant role of Ti–O interactions in controlling the intrinsic electronic properties of rhombohedral NBT. A quantitative comparison with previous first-principles studies further supports the reliability and novelty of the present results. Zeng et al. [20] reported that the conduction-band minimum of rhombohedral NBT is predominantly composed of Ti-3d states with minor Bi-6p contributions, while Lü et al. [21] observed similar orbital characteristics across different crystallographic phases. In the present work, the partial density of states reveals that Ti-3d orbitals contribute overwhelmingly to the conduction-band edge, whereas Bi-6p states mainly appear at higher energies, indicating a secondary role in low-energy electronic excitations. Compared with earlier studies, the present analysis explicitly correlates the enhanced Ti–O hybridization strength, as reflected by Mulliken bond populations, with increased band dispersion near the band edges. This quantitative linkage provides a more detailed microscopic interpretation of band-gap formation in rhombohedral NBT. Overall, the electronic structure analysis reveals that pristine $Na_{0.5}Bi_{0.5}TiO_3$ is a wide-band-gap, direct semiconductor in which strong Ti–O covalent interactions govern both the formation of the conduction-band edge and the dispersion of valence-band states. These features provide a crucial electronic foundation for understanding the optical absorption behavior discussed in Section 3.4 and establish a direct link between chemical bonding and optoelectronic response in rhombohedral NBT.

Table 2. Mulliken atomic charges population of NBT material.

Elements	Population					Charge (e)
	s	**p**	**d**	**f**	**Total**	
Bi	1.55	1.57	0.00	0.00	3.12	1.88
Na	2.11	6.04	0.00	0.00	8.16	0.84
Ti	2.36/2.38	s/6.63	2.18/2.21	0.00	11.17/11.20	0.80/0.83
O	1.85/1.86	4.87/4.88	0.00	0.00	6.72/6.73	-0.72/-0.73

Table 3. Mulliken bond population of NBT material.

Structure	**Bond**	**Population**	**Bond Length (Å)**	**Bond type**
NBT	Bi-O	0.05	2.3016	Covalence
	Na-O	0.03	2.4427	Covalence
	Ti(1)-O(1,3,5)	0.66	1.8526	Covalence
	Ti(2)-O(2,4,6)	0.59	1.8827	Covalence

3.3 Magnetic Properties

The magnetic properties of pristine rhombohedral $Na_{0.5}Bi_{0.5}TiO_3$ were examined using spin-polarized density functional theory calculations to verify the possible presence of intrinsic magnetism. Figure 5 presents the spin-resolved density of states (DOS) of NBT, in which the spin-up and spin-down components are nearly identical over the entire energy range. The almost perfect symmetry between the two spin channels indicates that rhombohedral NBT possesses a non-magnetic ground state. The calculated integrated spin density is extremely small and close to zero, confirming the absence of long-range magnetic ordering. Such negligible residual spin polarization originates from numerical asymmetry inherent in spin-polarized calculations and does not indicate intrinsic magnetism.

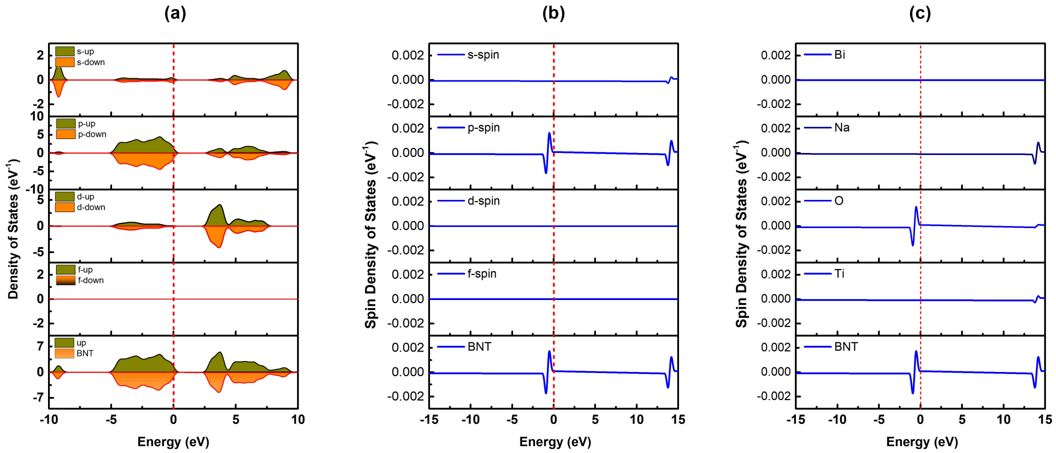

Figure 5. Decomposed density of states (a), spin density of states (b) and element spins of NBT (c).

Table 4. Integrated Spin Densities of NBT.

Material	**Integrated Spin Density**	**Integrated |Spin Density|**	**Magnetic Behavior**
NBT	0.3510×10^{-13}	0.6886×10^{-03}	Non-magnetic

Element-resolved analysis further reveals that none of the constituent atoms (Bi, Na, Ti, or O) exhibits a significant magnetic moment. In particular, the Ti-3d and O-2p states that dominate the valence and conduction bands remain completely spin-unpolarized. These results are consistent with previous experimental and theoretical studies, which consistently report that pristine $Bi_{0.5}Na_{0.5}TiO_3$ is intrinsically non-magnetic [16,35,37,42]. It is worth noting that magnetic behavior reported in some NBT-based systems is generally associated with extrinsic effects, such as defects, dopants, or surface states, rather than the intrinsic bulk properties of stoichiometric NBT. Therefore, the present results confirm that magnetic contributions do not play a role in the intrinsic electronic and optical properties of pristine rhombohedral NBT, justifying the focus on non-magnetic electronic structure in the subsequent analyses.

3.4 Optical Properties

The optical properties of rhombohedral $Na_{0.5}Bi_{0.5}TiO_3$ were investigated to elucidate the relationship between electronic structure, chemical bonding, and optical excitation mechanisms. Based on the optimized ground-state electronic structure, the frequency-dependent complex dielectric function was calculated within the linear response formalism, from which various optical constants were derived.

$$(\alpha h\nu)^n = A(h\nu - E_g) \quad (1)$$

where E_g is the bandgap energy of material,s **A** and **n** are constants, $h\nu$ is the photon energy with h is the Planck constant. The two possible value of n are: n = 2 for direct allowed transitions and n = 1/2 for indirect allowed transitions. Figure 6(a) shows the calculated optical absorption spectrum of NBT in the wavelength range from 200 to 800 nm. A clear absorption edge is observed at approximately 410 nm, which is in reasonable agreement with available experimental reports [9,44], considering the intrinsic limitations of standard GGA-based calculations. Strong absorption features are present in the ultraviolet region between 200 and 300 nm, whereas the absorption in the visible range is relatively weak, indicating that pristine NBT primarily responds to ultraviolet radiation.

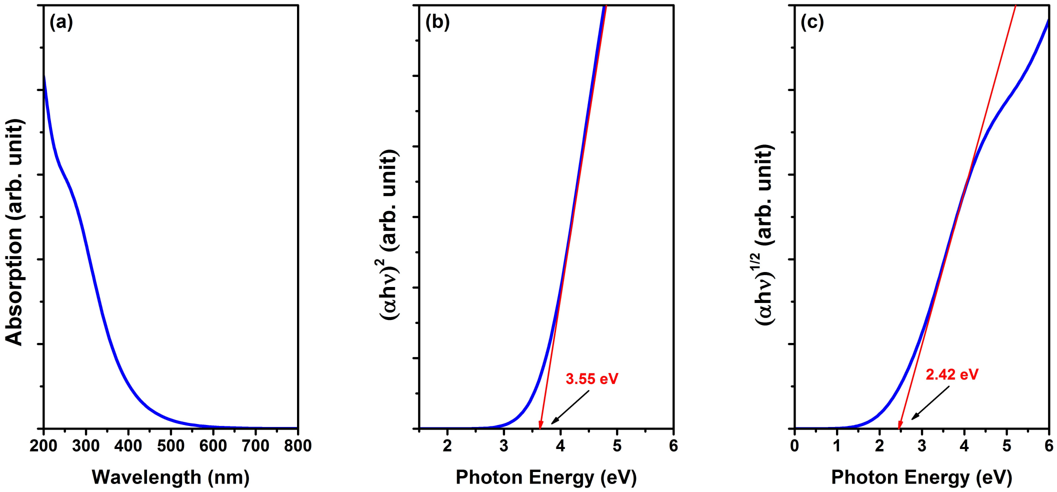

Figure 6. Absorption spectra of NBT (a) and Wood-Tauc plots for direct (b) and indirect allowed transitions (c).

To estimate the optical band gap, the Tauc method was applied assuming both direct and indirect allowed transitions. As shown in Figure 6b and Figure 6c, the extracted direct optical band gap is approximately 3.55 eV, while the indirect band gap is about 2.42 eV. The direct optical band gap is larger than the electronic band gap obtained from DFT calculations, which is a commonly observed feature in wide-band-gap oxides.

Table 5. Comparison table of the results.

Method	**Direct E_g (eV)**	**Indirect E_g (eV)**	**Reference**
GGA-PBE (this work)	3.55	2.42	This work
DFT-GGA	3.03	–	[20]
Experiment	~3.0	–	[38]

This discrepancy can be attributed to excitonic effects, optical transition selection rules, and the well-known underestimation of band gaps within the GGA-PBE framework. Importantly, the direct optical transition is consistent with the direct nature of the calculated electronic band structure.

$$n(\omega) = [\{\varepsilon_1^2(\omega) + \varepsilon_2^2(\omega)\}^{1/2} + \varepsilon_1(\omega)]^{1/2} \quad (2)$$

$$k(\omega) = (1/2^{1/2}).[\{\varepsilon_1^2(\omega) + \varepsilon_2^2(\omega)\}^{1/2} - \varepsilon_1(\omega)]^{1/2} \quad (3)$$

$$\alpha(\omega) = (2^{1/2}\omega/c).[\{\varepsilon_1^2(\omega) + \varepsilon_2^2(\omega)\}^{1/2} - \varepsilon_1(\omega)]^{1/2} \quad (4)$$

$$R(\omega) = [(\{\varepsilon_1(\omega) + i\varepsilon_2(\omega)\}^{1/2} - 1)/(\{\varepsilon_1(\omega) + i\varepsilon_2(\omega)\}^{1/2} - 1)/]^{1/2} \quad (5)$$

$$L(\omega) = \varepsilon_2(\omega)/[\varepsilon_1^2(\omega) + i\varepsilon_2^2(\omega)] \quad (6)$$

$$\sigma(\omega) = (\omega/4\pi i)[\varepsilon_1(\omega) + i\varepsilon_2(\omega) - 1] \quad (7)$$

where $\varepsilon_1(\omega)$ and $\varepsilon_2(\omega)$ are the real and imaginary parts of the dielectric function, $\omega = 2\pi\nu$ is the angular frequency of the incident light, c is the speed of light in the vacuum. The refractive index $n(\omega)$ represents for the polarization of light travelling through while the extinction coefficient $k(\omega)$ represents for the dissipation of energy in the material. The absorption coefficient $\alpha(\omega)$ show the dependence of the absorbance on the incident wavelength while the reflectivity $R(\omega)$ give the information on the reflected light. The loss function $L(\omega)$ give information on the amount of energy had loss and the optical conductivity $\sigma(\omega)$ illustrates the relationship between the external inducing electric field and internal induced current in the materials.

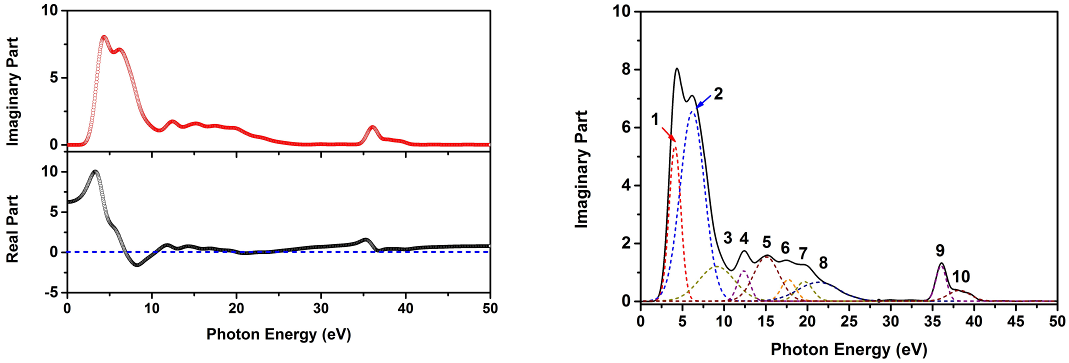

Figure 7. Dielectric functions (a) and peaks positions in the imaginary part of dielectric function of NBT (b).

Table 6. Peak positions in imaginary part of dielectric function of NBT

Peaks	**1**	**2**	**3**	**4**	**5**	**6**	**7**	**8**	**9**	**10**
Energy (eV)	4.10	6.19	6.33	12.36	15.08	17.71	19.63	21.32	36.03	38.20

The microscopic origin of the optical transitions can be understood by correlating the absorption features with the electronic density of states.

Importantly, the present analysis goes beyond previous optical studies by explicitly mapping the dominant peaks in the imaginary part of the dielectric function to specific orbital-resolved interband transitions and corresponding bond population characteristics, thereby providing a quantitative microscopic interpretation rather than a purely descriptive assignment.

Table 7. Assignment of major optical transitions in rhombohedral $Na_{0.5}Bi_{0.5}TiO_3$

Peak No.	**Energy (eV)**	**Dominant transition**	**Orbital origin**	**Physical interpretation**
1	~4.10	VB → CB	O-2p → Ti-3d	Fundamental optical absorption edge dominated by Ti–O covalent interaction
2	~6.19	VB → CB	O-2p → Ti-3d	Higher-energy interband transition within TiO_6 octahedra
3	~6.33	VB → CB	O-2p → Ti-3d / Bi-6p	Mixed Ti–O and Bi–O contributions
4	~12.36	Deep VB → CB	Bi-6s / O-2p → Ti-3d	Transitions involving deeper Bi-related states
5–7	15–22	Deep states → CB	Bi-6s / O-2s → Ti-3d / Bi-6p	High-energy electronic excitations
8–10	>30	Core-like transitions	O-2s / deeper states	Energy-loss dominated processes

To further clarify the microscopic origin of the optical response, the major peaks in the imaginary part of the dielectric function can be directly assigned to specific orbital-resolved interband transitions. The first low-energy peak around 4.1 eV mainly originates from transitions between O-2p states at the valence-band maximum and Ti-3d states at the conduction-band minimum, which dominate the optical absorption edge. Subsequent peaks in the range of 6–7 eV are associated with higher-energy O-2p to Ti-3d and Bi-6p transitions, reflecting the increasing contribution of Bi-related states at elevated energies. High-energy peaks above 12 eV arise from deeper electronic states, such as Bi-6s and O-2s orbitals, and therefore contribute primarily to energy-loss processes rather than practical optical absorption. This explicit assignment establishes a direct quantitative connection between chemical bonding, electronic structure, and optical excitation mechanisms in rhombohedral NBT. The absorption edge and the low-energy optical transitions mainly originate from electronic excitations from O-2p states in the valence band to Ti-3d states in the conduction band. This observation highlights the decisive role of Ti–O covalent interactions in governing the optical response of NBT, in agreement with the electronic structure and Mulliken population analyses discussed in Sections 3.2 and 3.3. Further insight into the optical behavior is provided by the calculated real and imaginary parts of the dielectric function, as shown in Figure 7(a). The static dielectric constant obtained from the real part of the dielectric function is approximately 6.61, which is consistent with previous theoretical studies [20]. The imaginary part of the dielectric function exhibits several pronounced peaks over a wide energy range, reflecting different interband transition processes, as shown in Table 6 and 7. The first three peaks at low energies are associated with transitions from O-2p states in the valence band to Ti-3d and Bi-6p states in the conduction band, corresponding to the dominant ultraviolet absorption features. Higher-energy peaks originate from deeper electronic states, such as Bi-6s and O-2s orbitals, and therefore mainly contribute to high-energy optical loss rather than practical photoresponse. Figure 8 presents other derived optical constants, including reflectivity, optical conductivity, refractive index, and energy-loss function. The reflectivity of NBT remains relatively low over a broad energy range, indicating good transparency outside the main absorption regions.

The static refractive index is approximately 2.57, consistent with the wide band gap of the material. The energy-loss function exhibits distinct peaks corresponding to collective plasma oscillations, suggesting potential applicability of NBT in ultraviolet and high-energy optical devices. Overall, the optical properties of rhombohedral $Bi_{0.5}Na_{0.5}TiO_3$ are governed by interband transitions dominated by Ti–O covalent interactions. By explicitly correlating electronic structure, chemical bonding, and optical spectra, the present results provide a coherent microscopic interpretation of the optical response of pristine NBT and offer valuable insight for the design of modified NBT-based materials with tailored optoelectronic properties.

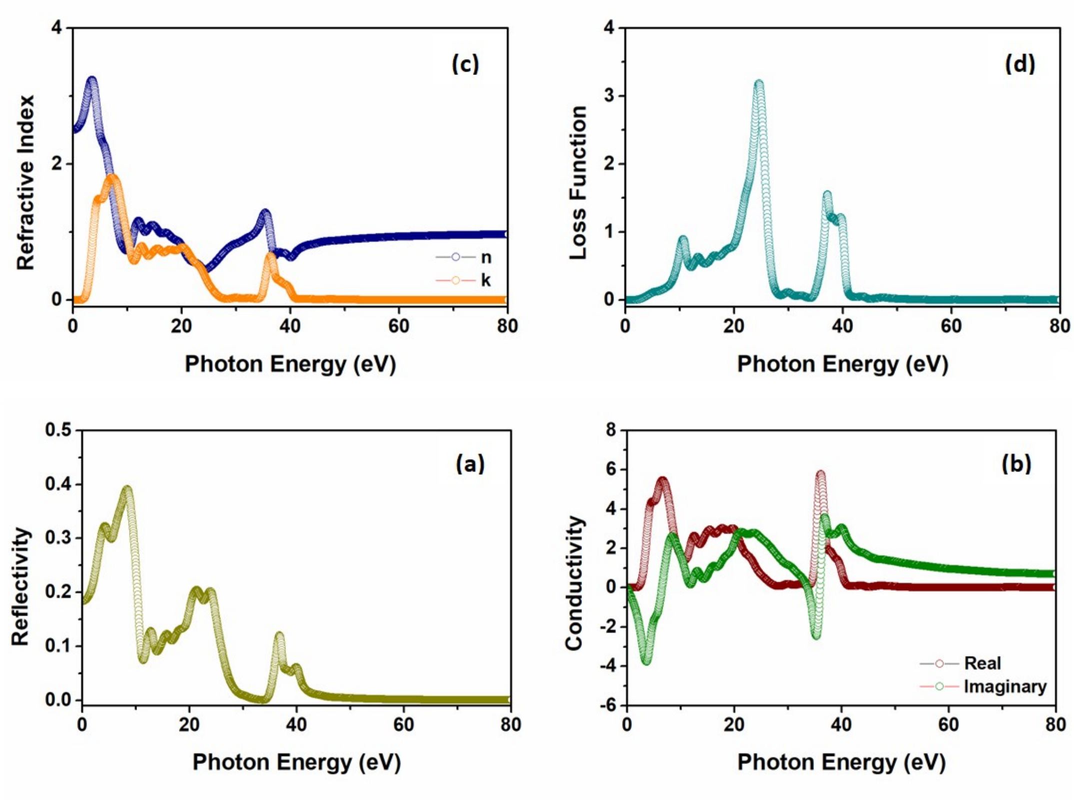

Figure 8. Reflectivity (a), conductivity (b), refractive index (c) and electron energy-loss spectrum (d) of NBT.

4. Conclusion

In this work, a comprehensive first-principles investigation of the structural, electronic, magnetic, and optical properties of rhombohedral $Na_{0.5}Bi_{0.5}TiO_3$ has been carried out using density functional theory within the GGA-PBE framework. The optimized structural parameters are in good agreement with available experimental data, confirming the stability of the rhombohedral R3c phase and the reliability of the adopted computational approach. Electronic structure calculations reveal that pristine NBT is a wide-band-gap direct semiconductor, with valence-band states dominated by O-2p orbitals and conduction-band states primarily derived from Ti-3d orbitals with minor Bi-6p contributions. Mulliken population analysis demonstrates a mixed ionic–covalent bonding nature, in which Ti–O bonds exhibit a pronounced covalent character. This strong Ti–O covalency plays a decisive role in shaping the band dispersion near the band edges and governing the formation of the conduction band. Spin-polarized calculations confirm that rhombohedral $Na_{0.5}Bi_{0.5}TiO_3$ is intrinsically non-magnetic, indicating that magnetic effects do not influence its fundamental electronic or optical behavior. Optical property analysis shows that NBT exhibits strong absorption in the ultraviolet region, with optical transitions mainly originating from O-2p to Ti-3d excitations. By explicitly correlating chemical bonding characteristics with electronic structure and optical response, this study establishes a unified microscopic interpretation of the intrinsic properties of pristine NBT.

More importantly, this work establishes a quantitative and unified microscopic link between chemical bonding, electronic band-edge formation, and optical excitation mechanisms in pristine rhombohedral $Na_{0.5}Bi_{0.5}TiO_3$. By explicitly correlating Mulliken bond populations, orbital-resolved density of states, and the energy positions of dominant dielectric-function peaks, the present study goes beyond previous isolated electronic or optical analyses. The insights provided herein offer a predictive framework for understanding how structural distortion or chemical modification can influence the optoelectronic properties of NBT-based materials, thereby serving as a reliable theoretical reference for future studies on doped or engineered NBT systems.

Funding: The authors declare that no funds, grants, or other support were received during the preparation of this manuscript.

Data Availability Statement: The data that support the findings of this study are available from the corresponding authors upon reasonable request.

Declaration of competing interest: The authors declare that they have no known competing financial interest or personal relationships that could have appeared to influence the work reported in this paper.

References

[1] Ș. Ţălu, L.V. Truong, N.T. Dung, (2025). Atomistic simulations of two dimensional materials: Insights from first principles and molecular dynamics methods, Journal of Nanomaterials and Applications. 1(1), 17–32. https://doi.org/10.65273/hhit.jna.2025.1.1.17-32.

[2] G. A. Smolenskii, A. I. Agranovskaya, (1961). New ferroelectrics of complex composition. IV. Soviet Physics-Solid State, 2, 2651-2654.

[3] J. Suchanicz, J. Kwapulinski, (1995). X-ray diffraction study of the phase transitions in $Na_{0.5}Bi_{0.5}TiO_3$. Ferroelectrics, 165 (1), 249-253. https://doi.org/10.1080/00150199508228304

[4] S. B. Vakhrushev et al., (1985). Phase transitions and soft modes in sodium bismuth titanate. Ferroelectrics, 63 (1), 153-160. https://doi.org/10.1080/00150198508221396

[5] S.-E. Park, S.-J. Chung, and I.-T. Kim, (1996). Ferroic Phase Transitions in $(Na_{1/2}Bi_{1/2})TiO_3$ Crystals. Journal of the American Ceramic Society, 79 (5), 1290-1296. https://doi.org/10.1111/j.1151-2916.1996.tb08586.x

[6] T. Takenaka, K.-i. M. Kei-ichi Maruyama, and K. S. Koichiro Sakata, (1991). $(Bi_{1/2}Na_{1/2})TiO_3$-$BaTiO_3$ System for Lead-Free Piezoelectric Ceramics. Japanese Journal of Applied Physics, 30 (9S), 2236. https://doi.org/10.1143/JJAP.30.2236

[7] J. Li et al., (2009). In situ self-assembly synthesis and photocatalytic performance of hierarchical $Bi_{0.5}Na_{0.5}TiO_3$ micro/nanostructures. Journal of Materials Chemistry, 19 (15). https://doi.org/10.1039/B816823G

[8] L. Wang, W. Wang, (2012). Photocatalytic hydrogen production from aqueous solutions over novel $Bi_{0.5}Na_{0.5}TiO_3$ microspheres. International Journal of Hydrogen Energy, 37 (4), 3041-3047. https://doi.org/10.1016/j.ijhydene.2011.10.105

[9] V. T. Lam et al., (2022). Design and optical properties of a new binary $Bi_{1/2}Na_{1/2}TiO_3$-$Eu_{1/2}Na_{1/2}TiO_3$ solid solution system. Optical Materials, 134. https://doi.org/10.1016/j.optmat.2022.113083

[10] G., Jagło, K., Kluczewska-Chmielarz, J., Suchanicz et al, (2025). New insights into structural, optical, electrical and thermoelectric behavior of $Na_{0.5}Bi_{0.5}TiO_3$ single crystals. Scientific Reports, 15, 2733, https://doi.org/10.1038/s41598-025-86625-4

[11] B. Parija et al., (2013). Structural and electromechanical study of $Bi_{0.5}Na_{0.5}TiO_3$-$BaTiO_3$ solid-solutions. Processing and Applications of Ceramics, 7 (2), 73-80. https://doi.org/10.2298/PAC1302073P

[12] K. Reichmann, A. Feteira, and M. Li, (2015). Bismuth Sodium Titanate Based Materials for Piezoelectric Actuators. Materials (Basel), 8 (12), 8467-8495. https://doi.org/10.3390/ma8125469

[13] N. H. Thoan et al., (2022). Fabrication and Optical Properties of $(1-x)Bi_{\frac{1}{2}}Na_{\frac{1}{2}}TiO_{3-x}Er_{\frac{1}{2}}Na_{\frac{1}{2}}TiO_3$ Solid Solution System. Journal of Electronic Materials, 52 (2), 1564-1574. https://doi.org/10.1007/s11664-022-10134-7

[14] J. Anthoniappen et al., (2015). Raman spectra and structural stability in B-site manganese doped $(Bi_{0.5}Na_{0.5})_{0.925}Ba_{0.075}TiO_3$ relaxor ferroelectric ceramics. Journal of the European Ceramic Society, 35 (13), 3495-3506. https://doi.org/10.1016/j.jeurceramsoc.2015.05.002.

[15] W. Chatta et al., (2019). TB-mBJ Calculations of Structural and Optoelectronic Properties of the Rhombohedral Phase of Bismuth Sodium Titanate $(Bi_{0.5}Na_{0.5})TiO_3$. Solid State Phenomena, 297, 165-172.
https://doi.org/10.4028/www.scientific.net/SSP.297.165

[16] D. D. Dung et al., (2022). Synthesis and Characterization of $(1-x)Bi_{1/2}Na_{1/2}TiO_{3+x}SrNiO_{3-\delta}$ Solid Solution System. Journal of Electronic Materials, 51 (6), 2716-2731. https://doi.org/10.1007/s11664-022-09534-6s

[17] M. Ogino et al., (2014). Polarization Rotation and Monoclinic Distortion in Ferroelectric $(Bi_{0.5}Na_{0.5})TiO_3$–$BaTiO_3$ Single Crystals under Electric Fields. Crystals, 4 (3), 273-295. https://doi.org/10.3390/cryst4030273.

[18] M., Bousquet, J.-R., Duclère, E., Orhan, A., Boulle, C., BacheletC, Champeaux, (2010). Optical properties of epitaxial $Na_{0.5}Bi_{0.5}TiO_3$ thin films: Experimental approach and density functional theory calculations. Journal of Applied Physics, 107, 10, 104107, https://doi.org/10.1063/1.3400095

[19] W. Zhao et al., (2014). Large strains accompanying field-induced ergodic phase-polar ordered phase transformations in $Bi(Mg_{0.5}Ti_3)O_3$-$PbTiO_3$-$(Bi_{0.5}Na_{0.5})TiO_3$ ternary system. Journal of the European Ceramic Society, 34 (10), 2299-2309. https://doi.org/10.1016/j.jeurceramsoc.2014.01.040

[20] M. Zeng, S. W. Or, and H. L. W. Chan, (2010). First-principles study on the electronic and optical properties of Na0.5Bi0.5TiO3 lead-free piezoelectric crystal. Journal of Applied Physics, 107 (4).
https://doi.org/10.1063/1.3309407

[21] H. Lü, S. Wang, and X. Wang, (2014). The electronic properties and lattice dynamics of $(Na_{0.5}Bi_{0.5})TiO_3$: From cubic to tetragonal and rhombohedral phases. Journal of Applied Physics, 115 (12).
https://doi.org/10.1063/1.4869733

[22] N. H. Linh et al., (2019). Alkali metal-substituted bismuth-based perovskite compounds: A DFT study. Journal of Science: Advanced Materials and Devices, 4 (3), 492-498.
https://doi.org/10.1016/j.jsamd.2019.06.005

[23] J. Baedi, et al. (2015). Study of electronic and optical properties of $Bi_{0.5}Na_{0.5}TiO_3$ crystals using full-potential LAPW method. Optik, 126, 1505–1509, https://doi.org/10.1016/j.ijleo.2014.04.092

[24] A., Deyneka, J., Suchaneck et al. (2015). Optical ellipsometry and Raman scattering study of $Na_{0.5}Bi_{0.5}TiO_3$-$_{7\%}BaTiO_3$ single crystals. Journal of Applied Physics, 117, 224103, Doi: 10.1063/1.4922133

[25] M. D. Segall et al., (2002). First-principles simulation: ideas, illustrations and the CASTEP code. J. Phys. Condens. Matter, 14, 2717-2744. https://doi.org/10.1088/0953-8984/14/11/301

[26] G. O. Jones, P. A. Thomas, (2002). Investigation of the structure and phase transitions in the novel A-site substituted distorted perovskite compound $Na_{0.5}Bi_{0.5}TiO_3$. Acta Crystallogr B, 58 (Pt 2), 168-78.
https://doi.org/10.1107/S0108768101020845

[27] J. P. Perdew et al., (1992). Atoms, molecules, solids, and surfaces: Applications of the generalized gradient approximation for exchange and correlation. Phys. Rev. B, 46 (11).
https://doi.org/10.1103/PhysRevB.46.6671

[28] J. P. Perdew, K. Burke, and M. Ernzerhof, (1996). Generalized Gradient Approximation Made Simple. Phys. Rev. Lett., 77 (18), 4. https://doi.org/10.1103/PhysRevLett.77.3865

[29] D. Vanderbilt, (1990). Soft self-consistent pseudopotentials in a generalized eigenvalue formalism. Physical Review B, 41 (11), 7892-7895. https://doi.org/10.1103/PhysRevB.41.7892

[30] C. G. Broyden, (1970). The Convergence of a Class of Double-rank Minimization Algorithms 1. General Considerations. IMA Journal of Applied Mathematics, 6 (1), 76-90.

https://doi.org/10.1093/imamat/6.1.76

[31] R. Fletcher, (1970). A new approach to variable metric algorithms. The Computer Journal, 13 (3), 317-322. https://doi.org/10.1093/comjnl/13.3.317

[32] D. Goldfarb, (1970). A Family of Variable-Metric Methods Derived by Variational Means. Mathematics of Computation, 24 (109), 23-26. 10.1090/S0025-5718-1970-0258249-6

[33] D. F. Shanno, (1970). Conditioning of Quasi-Newton Methods for Function Minimization. Mathematics of Computation, 24 (111), 647-656. Doi: 10.1090/S0025-5718-1970-0262289-9

[34] H. J. Monkhorst, J. D. Pack, (1976). Special points for Brillouin-zone integrations. Phys. Rev. B, 13 (12). https://doi.org/10.1103/PhysRevB.13.5188

[35] D. D. Dung et al., (2022). Structural, optical, and magnetic properties of a new complex $(1-x)Bi_{1/2}Na_{1/2}TiO_{3+x}MgNiO_{3-\delta}$ solid solution system. Applied Physics A, 128 (2). https://doi.org/10.1007/s00339-021-05255-5

[36] D. D. Dung, N. T. Hung, and D. Odkhuu, (2019). Structure, optical and magnetic properties of new $Bi_{0.5}Na_{0.5}TiO_3$ $SrMnO_3$-delta solid solution materials. Sci Rep, 9 (1), 18186. https://doi.org/10.1038/s41598-019-54172-4

[37] D. D. Dung et al., (2022). Magnetic properties of new $(1-x)Bi_{1/2}Na_{1/2}TiO_{3+x}BaNiO_{3-\delta}$ solid solution materials. Applied Physics A, 128 (2). https://doi.org/10.1007/s00339-022-05281-xs

[38] A. Franco, P. Banerjee, and P. L. Romanholo, (2018). Effect of composition induced transition in the optical band-gap, dielectric and magnetic properties of Gd doped $Na_{0.5}Bi_{0.5}TiO_3$ complex perovskite. Journal of Alloys and Compounds, 764, 122-127. Doi: 10.1016/j.jallcom.2018.03.022

[39] D. D. Dung et al., (2022). Magnetic Properties of a $(1-x)Bi_{0.5}Na_{0.5}TiO_{3+x}CaNiO_{3-\delta}$ Solid Solution System Prepared by Sol–Gel Technique. Journal of Electronic Materials, 51 (5), 1905-1921. https://doi.org/10.1007/s11664-022-09457-2.

[40] R. S. Mulliken, (1955). Electronic Population Analysis on LCAO-MO Molecular Wave Functions. I. The Journal of Chemical Physics, 23 (10), 1833. https://doi.org/10.1063/1.1740588

[41] R. Carbó-Dorca, P. Bultinck, (2004). Quantum Mechanical Basis for Mulliken Population Analysis. Journal of Mathematical Chemistry, 36 (3), 231-239. https://doi.org/10.1023/B:JOMC.0000044221.23647.20.

[42] D. D. Dung et al., (2021). Optical properties of a new $(1-x)Bi_{1/2}Na_{1/2}TiO_{3+x}Pr_{1/2}Na_{1/2}TiO_3$ solid solution system. Materials Letters, 302. https://doi.org/10.1016/j.matlet.2021.130381s

[43] J. Goldsby et al., (2015). First-Principle and Experimental Study of a Gadolinium-Praseodymium-Cobalt Pseudobinary Intermetallic Compound. Journal of Materials, 2015, 1-9. https://doi.org/10.1155/2015/753612

[44] D. D. Dung et al., (2022). Fabrication and optical properties of new $(1-x)Bi_{1/2}Na_{1/2}TiO_{3+x}Ho_{1/2}Na_{1/2}TiO_3$ solid solution materials. Optical Materials, 132. https://doi.org/10.1016/j.optmat.2022.112750

[45] D. L. Wood, J. Tauc, (1972), Weak Absorption Tails in Amorphous Semiconductors.s Physical Review B, 5 (8), 3144-3151. https://doi.org/10.1103/PhysRevB.5.3144

[46] V. T. Lam et al., (2022). Surface ferromagnetism of complex defects lead-free ferroelectric $Bi_{0.5}Na_{0.5}TiO_3$ materials. Surface and Interface Analysis, 55 (4), 243-255. https://doi.org/10.1002/sia.7184

[47] B. Luo et al., (2015). Electronic structure, optical and dielectric properties of $BaTiO_3/CaTiO_3/SrTiO_3$ ferroelectric superlattices from first-principles calculations. Journal of Materials Chemistry C, 3 (33), 8625-8633. https://doi.org/10.1039/C5TC01622C

[48] X. D. Zhang et al., (2008). First-principles study of electronic and optical properties in wurtzite $Zn_{1-x}Cd_xO$. Journal of Applied Physics, 103 (6), 063721. https://doi.org/10.1063/1.2901033.